electronics

MDPI

Article

A 220 GHz Traveling-Wave Tube Based on a Modified Staggered Double Corrugated Waveguide

Weihua Ge * and Sheng Yu

School of Electronic Science and Engineering, University of Electronic Science and Technology of China, Chengdu 611731, China

* Correspondence: 201911022224@std.uestc.edu.cn

Abstract: Staggered double-grating slow-wave structures (SDG-SWSs), which are easy to fabricate and have broadband characteristics, play a core role in research on high-power terahertz (THz) traveling-wave tubes (TWTs). However, their relatively low interaction impedance restricts further improvements in the output power of SDG-TWTs. A modified staggered double corrugated waveguide (MSDCW) SWS that evolved from a staggered double corrugated waveguide (SDCW) SWS is proposed in this study for the first time. The MSDCW-SWS has both the advantages of a wide bandwidth and a high interaction impedance. The width of the beam tunnel also has little effect on the lower cutoff frequency. High-frequency calculations reveal that the passband of the MSDCW-SWS is 10 GHz wider than that of the SDG-SWS, and the interaction impedance is about 1.34 ohm higher than that of the SDG-SWS and 1.07 ohm higher than that of the SDCW-SWS at 220 GHz when the dispersion is the same. The results of the interaction simulation show that the MSDCW-TWT has a maximum gain of ~22.11 dB with a maximum output power of ~117 W and a maximum electron efficiency of ~2.64% at 220 GHz with an electron beam of 24.6 kV and 180 mA. The MSDCW should therefore be considered as a promising SWS for high-power and wideband THz traveling-wave amplification.

Keywords: traveling-wave tube (TWT); modified staggered double corrugated waveguide (MSDCW); terahertz (THz); slow-wave structure (SWS); sheet beam

Citation: Ge, W.; Yu, S. A 220 GHz Traveling-Wave Tube Based on a Modified Staggered Double Corrugated Waveguide. *Electronics* **2024**, *13*, 4483. https://doi.org/10.3390/electronics13224483

Academic Editors: Federico Alimenti and Djuradj Budimir

Received: 22 October 2024
Revised: 7 November 2024
Accepted: 12 November 2024
Published: 15 November 2024

1. Introduction

Terahertz (THz) technology has enormous potential due to THz waves' high penetrability, broadband characteristics, strong absorption, low energy, and so on [1]. In the field of chemistry, a terahertz wave is fired to observably increase the selectivity and conductance of Ca^{2+} [2]. For biological medicine and treatment, it has been proven that a terahertz stimulus at 44 THz can efficiently facilitate the unwinding process for DNA duplexes [3]. In addition, a terahertz imaging system is established in [4]. Vacuum electronic devices (VEDs) are the core components of important systems such as radar, satellites, space communication, and medical treatment [5,6]. VEDs are often designed as terahertz sources to obtain terahertz waves [7]. A traveling-wave tube (TWT) is one of the most significant amplifiers because of its high power, broad bandwidth, and high power capacity [8,9]. The main process of input signal amplification (beam–wave interaction) is facilitated in the slow-wave structure (SWS), so the SWS determines the signal amplification ability of the TWT. The prominent advantage of a helix SWS is its broad bandwidth, which is also a key factor considered in the application of helix TWT amplifiers [10,11]. However, as the operating frequency band of TWTs rises to the THz band, the difficulty of fabrication increases for the helix SWS due to structural limitations [12]. The advantage of a coupled-cavity SWS is its high-power output [13,14]. However, it is commonly not researched in higher-frequency bands due to its structural complexity. For these reasons, in current studies on TWTs, SWSs with broad operating frequency bands that are simple to manufacture are explored. At present, folded

waveguide (FW) and staggered double-grating (SDG) structures meet these criteria and are mainly used as SWSs, forming circuits for THz-TWT. A 220 GHz FW-TWT has an output power of 20 W and a corresponding bandwidth of 10 GHz [15]. In simulations, an output power of over 55.1 W from 230 to 280 GHz for an SDG-TWT has been obtained [16].

The size reduction in SWSs operating at higher frequency bands also brings about a size reduction in electron beams, which also means that the output power of the TWT will be greatly reduced. By replacing a circular beam with a sheet beam, the beam area can be enlarged to obtain a relatively greater current. Therefore, an SDG-TWT with a rectangular beam generally produces a higher output power than an FW-TWT with a circular beam [17]. However, the relatively low interaction impedance of SDG-SWSs limits the efficiency of the interaction between the electromagnetic (EM) wave supported by the structure and beam in SDG-TWTs. Therefore, it is challenging to improve the interaction impedance of SWSs to obtain a higher output power of TWTs. An improved SWS with a beam tunnel with a curved profile has been demonstrated to increase the interaction impedance [18]. A TWT based on a novel helical groove rectangular SWS has a higher gain and electron efficiency in [19]. A chevron-shaped double-staggered grating waveguide with a higher interaction impedance and a low phase velocity has been proposed and researched [20]. Recently, a staggered double corrugated waveguide (SDCW) SWS with the advantages of the high coupling impedance of a symmetrical double-grating SWS and the wide operating band of an SDG-SWS has been proposed [21,22]. The bandwidth of the SDCW-SWS is 10 GHz wider than that of the SDG-SWS, and the coupling impedance at 195 GHz is 62% higher than that of the SDG-SWS.

In this article, a novel *modified staggered double corrugated waveguide* (MSDCW) *slow-wave structure* (SWS) is proposed to further improve the performance of SWS in terms of interaction impedance and related performance parameters in comparison to those of an SDCW-SWS. The simulation results show that the MSDCW-SWS has a wider bandwidth than the SDG-SWS and a higher interaction impedance than the SDCW-SWS when the dispersion is same. The particle-in-cell (PIC) simulation results of an MSDCW-TWT show that the output power and passband of the MSDCW-TWT are higher than those of the corresponding TWT based on the SDG-SWS.

2. Methods and Models

2.1. Model of the SWSs

The traditional SDG-SWS and the recently proposed SDCW-SWS are exhibited in Figure 1a,b. As described in [22], the evolution of SDG-SWS to SDCW-SWS is shown. The gratings of SDG-SWS, as shown in Figure 1a, extend to the beam tunnel, which has a width of *a* along y-axis and a height of *b* along x-axis. Then along the *x-o-z* plane of SDCW-SWS, a groove is developed to produce a new tunnel through which electrons can be propagated. It is this change that allows SDCW to have both the qualities of SDG and symmetrical double grating.

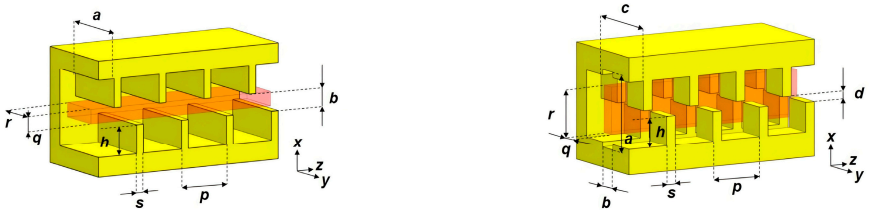

(**a**) (**b**)

Figure 1. Schematic diagrams with sheet beams (red regions) of (**a**) the traditional SDG-SWS; (**b**) the proposed SDCW-SWS.

To more clearly describe the MSDCW-SWS evolved from SDCW-SWS, a schematic figure of MSDCW-SWS is shown separately in Figure 2. On the basis of SDCW-SWS, a

ridge with a width of W_r, a height of H_g, and a thickness along the z-axis of S_r is loaded along the x-o-z plane of the MSDCW-SWS at the end of each grating near the electron beam channel. The ridge intersecting vertically with each grating of SDCW-SWS right next to the original electron beam channel is a key factor that means that all ridges and gratings together have the same dimensional parameter b of the beam channel.

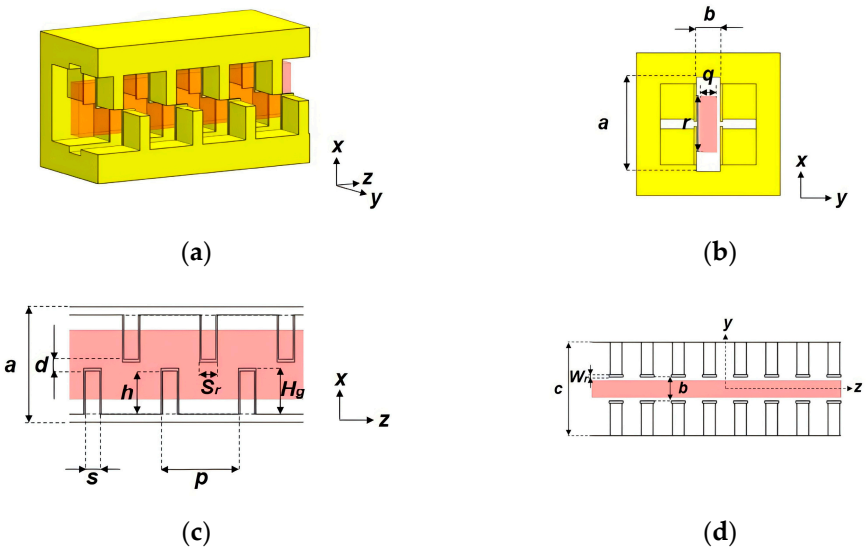

Figure 2. (**a**) Schematic diagram; (**b**) left view; (**c**) front view; (**d**) top view with a sheet beam (red region) of the MSDCW-SWS.

Both rows of ridge-loaded gratings, which are staggered about middle plane, x-o-z, in Figure 2c, play a key role in strengthening the axial electric field compared with the gratings without the added ridges of SDCW-SWS. Moreover, both rows of ridge-loaded gratings that are symmetrical around the y-o-z plane also enhance the axial electric field compared to the gratings without the added ridges of SDCW-SWS, which shows that the MSDCW-SWS has further strengthened the coupling impedance in top view of the symmetrical double-grating SWS (Figure 2d). Meanwhile, the peculiarity of the MSDCW-SWS is that the upper-side corrugations are shifted with respect to the lower-side corrugations, which ensure the EM energy is concentrated mainly within the beam tunnel, losses are reduced, and energy is facilitated for transmission. Only by slightly changing the dimensional parameter c of the MSDCW-SWS after being developed from the SDCW-SWS can the coupling impedance be greatly improved for a greater interaction between EM wave and beam based on the same conditions. Analogously, the MSDCW-SWS also retains other advantages of SDCW-SWS over SDG-SWS, such as wider bandwidth. The dimension a in Figure 2 merely represents the width of tunnel and has little effect on the change in lower cutoff frequency according to the value of c. This characteristic means that the area of the electron-propagating channel of the MSDCW-SWS can be increased by extending dimension a without changing the dispersion to further enlarge electron beam area to obtain larger current. This will be proven in the subsequent analysis.

To fulfil the synchronized dispersion condition to make a fair comparison, the optimized parameters of all dimensions of the three SWSs are given in Table 1 using simulation calculations. Most of the parameters of dimensions for the SDCW-SWS and SDG-SWS are exactly the same as those in [22,23], respectively. Other parameters of dimensions are slightly different to ensure the same frequency range of operation and same phase velocity for the three structures.

Table 1. Optimized parameters of the MSDCW-SWS, SDCW-SWS, and SDG-SWS.

Parameter	Value (μm)		
	MSDCW-SWS	**SDCW-SWS**	**SDG-SWS**
Structure size			
p	530	530	530
s	100	100	80
h	300	300	300
W_r	20		
H_g	320		
S_r	120		
d	80	80	
c	800	840	
Tunnel size			
b	200	200	200
a	790	790	790
Beam size			
r	520	520	520
q	140	140	140

Remarkably, the fabrication method adopting nano-computer numerical control (CNC) milling techniques of MSDCW-SWS is the same as that of the SDCW-SWS and the SDG-SWS [24,25]. This means that the MSDCW-SWS is as easy to fabricate as SDG-SWS. The MSDCW-SWS can be split into two halves along the *x*-*o*-*z* plane through the beam tunnel center. MSDCW-SWS can be divided by etching a groove on a copper block. The two split halves can be assembled together for fabrication and assembling process.

2.2. Whole Transmission and Interaction Model of the MSDCW-TWT

As shown in Figure 3, the full high-frequency and interaction structure of the MSDCW-TWT is shown, consisting of SWS circuit, which includes multiple vacuum models of MSDCW-SWS, gradual SWSs, the beam tunnel, and mode convertors. Gradual SWSs and mode convertors together operate as coupling devices that facilitate the process of coupling signals into and out of the interaction circuits to enhance the power of the wave by interacting with the beam. The period numbers of SWS circuit and gradual SWSs are 62 periods and 5 periods for each gradual section, respectively. In the gradual SWSs, which can control reflection at a relatively low level within a broadband, the height and thickness of gratings gradually change in fixed proportion, respectively. The mode converter plays a role in converting the TE_{10} mode for rectangular waveguide to the operating mode TE_{11} of the MSDCW-SWS. The signal input port is port 1, and the signal output port is port 2. The port on the beam tunnel near the electron gun is port 3, and the port at the other end near the collector is port 4.

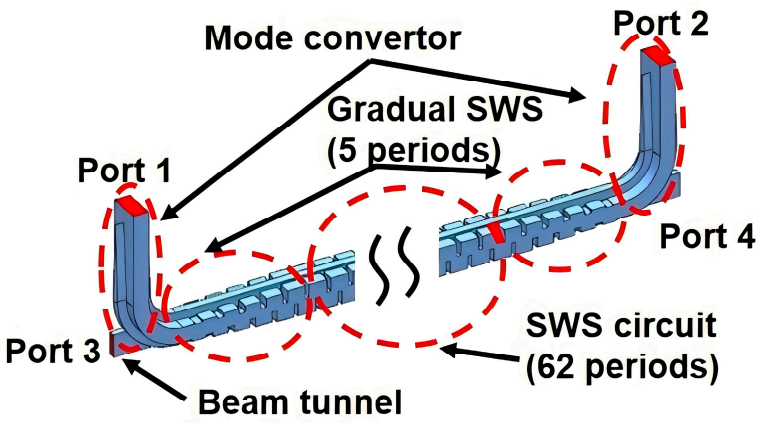

Figure 3. Vacuum model of the MSDCW-TWT.

2.3. Materials of Models and Methods of Research

In view of the surface roughness of the material and operating frequency band, the material used in all above models is copper with a conductivity of 2×10^7 S/m [19,20]. The high-frequency characteristics of MSDCW-SWS, SDCW-SWS, and SDG-SWS, such as dispersion and coupling impedances, are calculated and summarized in Section 3.1. The 3D EM simulation software Ansys HFSS 2020 and CST STUDIO SUITE 2020 enable visual modeling and automatic parameter sweeping calculations. HFSS is generally used to calculate high-frequency characteristics. CST can be applied in calculations of high-frequency characteristics of SWSs, transmission parameters, and interaction of TWTs. In brief, different kinds of simulations are conducted in different software due to their computing applications and in order to mutually verify the performance of SWSs. In subsequent studies, HFSS with master–slave boundary is used to calculate the high-frequency characteristics of SWSs, including normalized phase velocity, electric field on the z-axis (E_z), and interaction impedance. A typical problem is that in order to ensure the accuracy of the calculation, the maximum number of passes is at least 20 over the adaptive solution, and once these have been completed, the adaptive analysis stops. Moreover, the maximum delta frequency per pass is less than 0.1%, and the basis functions should be set to mixed order.

A quasi-analytical solution for these SWSs based on rectangular gratings can be found in [26,27]. The coupling impedance characterizes the effective degree of interaction between EM wave and electron beam in SWSs. In particular, the electron beam interacts with the longitudinal electric field of SWSs in TWTs. For these reasons, expression of coupling impedance is as follows:

$$K_c = \frac{E_z^2}{2\beta^2 P}. \quad (1)$$

Here, E_z is the electric field on the z-axis, P is the power flow, and β is propagation constant. It is clear that the coupling impedance is to a great extent determined by the value of E_z, which makes the subsequent comparison of E_z values meaningful.

In Section 3.2, transmission parameters are calculated in CST Microwave Studio (CST MWS) 2020. It is also typical that in order to ensure the precision accuracy of the calculation, the accuracy selection in the solver settings should be at least -40 dB and the minimum mesh step should be less than 0.01. On the basis of the above calculations, simulation of the interaction in Section 3.3 is conducted in CST Particle Studio 2020. A typical problem in this subsection is that the number of macroparticles should exceed about 712 to ensure convergence of the results. Under synchronous conditions, the predicted optimum voltage of the two TWTs operating at 220 GHz is 24.6 kV. The dimensions of cross-section for sheet electron beam with current of 180 mA are set to 0.52 mm $\times$ 0.14 mm, which indicates a 46% filling ratio. The input signal powers are both set to 0.72 W, and the values for uniform magnetic field, which can be generated by solenoidal winding for beam focusing, are both 1.1 T. In consideration of the distribution loss of entire system, the conductivities of copper material of the circuits are set to 2×10^7 S/m.

3. Results

3.1. High-Frequency Characteristics of the SWSs

The dispersion, E_z, and coupling impedance values shown in Figures 4 and 5 are obtained by calculations using the parameters of dimensions listed in Table 1. As shown in Figure 4a, the values of the phase velocity for all the SWSs calculated using HFSS are same in the operating bandwidths, which means the SWSs have the same synchronous voltage as that in the precondition for the comparison of subsequent PIC results. Meanwhile, the MSDCW-SWS has a broad passband of ~90 GHz from 194 to 284 GHz, which is 1 GHz more than for the SDCW-SWS (~89 GHz; 192~281 GHz) and 10 GHz more than for the SDG-SWS (~80 GHz; 189.5~269.5 GHz). This indicates that the passband of the MSDCW-SWS is at least not worse than that of the SDCW-SWS, which is the basis for the subsequent comparison of coupling impedance values. According to the flat range of the curve, the

operating frequency band of the MSDCW-SWS can be preliminarily predicted to be 200~250 GHz, which is the range used in the subsequent comparison.

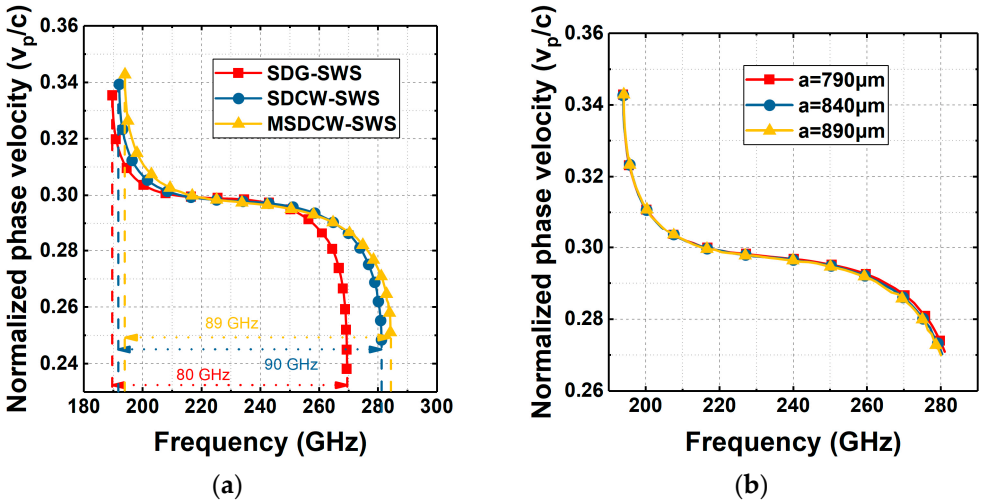

Figure 4. Normalized phase velocity versus frequency calculated using HFSS (**a**) for the MSDCW-SWS, SDCW-SWS, and SDG-SWS; (**b**) for the MSDCW-SWS when dimension *a* is set to 790, 840, and 890 μm.

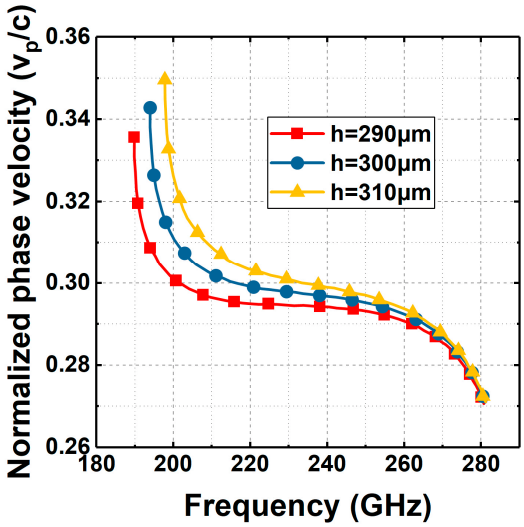

Figure 5. Normalized phase velocity versus frequency calculated using HFSS for the MSDCW-SWS when dimension *h* is set to 290, 300, and 310 μm.

Figure 4b reveals that the phase curves are almost at the same level when dimension *a* of the MSDCW-SWS is set to 790, 840, and 890 μm, respectively, which verifies that the dispersion characteristics of the MSDCW-SWS are unaffected by the changes in the width of the tunnel, differing from the SDG-SWS. Nevertheless, the sizes of parameter *a* of the three structures are kept consistent to make a fair comparison. In addition, the influence of parameter *h* on the phase velocity is analyzed. As can be seen in Figure 5, as parameter *h* increases from 290 to 310 μm, the bandwidth narrows and the phase velocity increases (especially near low cutoff frequencies).

Figure 6a displays the electric field on the *z*-axis (E_z) of the three SWSs. The E_z values can be ordered from highest to lowest as follows: the MSDCW-SWS, the SDCW-SWS, and the SDG-SWS. One reason for this is that the protruding part of the MSDCW-SWS further reduces the distance between the two staggered gratings of the SDCW-SWS along the *x*-axis on the basis of *d* in the middle plane, *x*-*o*-*z*, as shown in Figure 2. Another reason is that

the protruding part of the MSDCW-SWS brings the two ridges along the *z*-axis closer than the two gratings along the *z*-axis of the SDCW-SWS in the middle plane, *y*-*o*-*z*. In brief, the protruding part of the ridges in both directions produces a larger E_z value compared with the values of the SDCW-SWS and SDG-SWS.

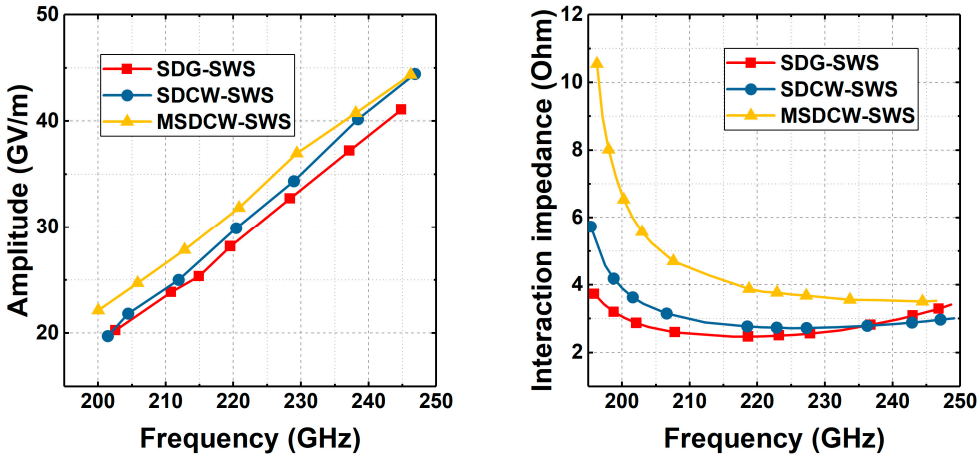

Figure 6. (**a**) Electric field E_z; (**b**) interaction impedance of the MSDCW-SWS, SDCW-SWS, and SDG-SWS calculated using HFSS.

In this work, comparisons of the interaction impedance for the three SWSs are discussed. As seen in Figure 6b, the interaction impedances of the MSDCW-SWS computed on the central axis of the beam tunnel are much larger than those of the SDCW-SWS and the SDG-SWS over the operating frequency band. In particular, the interaction impedance of the MSDCW-SWS at 220 GHz is 3.83 ohm (1.07 ohm higher than the SDCW-SWS and 1.34 ohm higher than the SDG-SWS), while that of the SDCW-SWS is 2.76 ohm and that of the SDG-SWS is 2.49 ohm. These results also confirm that the E_z of the MSDCW-SWS is further strengthened compared to the SDCW-SWS and SDG-SWS. With the improvement of the coupling impedance, the MSDCW-TWT should have higher-efficiency beam–wave energy exchange.

3.2. Transmission Parameters of the TWTs

The optimized S parameters for the whole circuit of the MSDCW-TWT are simulated using CST MWS, optimized, and analyzed. Simultaneously, the various parameters of the SDG-TWT, which is a traveling wave amplifier frequently used as a signal amplification device, are designed and analyzed in order to further prove the advantages of the MSDCW-TWT. As shown in Figure 7a, the reflection parameter S_{11} for the MSDCW-TWT and SDG-TWT is lower than −15 dB from 201 to 247 GHz and from 202 to 245 GHz, respectively, which shows the TWTs have good coupling and matching performances within the whole system. Figure 7b shows that the attenuation parameter S_{21} of the MSDCW-TWT and SDG-TWT is lower than −3.4 dB from 201 to 247 GHz and from 202 to 245 GHz, respectively. Table 2 lists the S parameters of the proposed MSDCW-TWT and other TWTs based on the SWSs evolved from SDG-SWSs operating at around 220 GHz in the literature. Under the premise that the frequency range difference for $S_{11} < -15$ dB is not large, the number of periods of the main SWSs greatly affects S_{21}. The above results prove the good transmission characteristics of the two TWT structures and show the reliability of the comparison of the PIC simulation results under approximately similar preconditions.

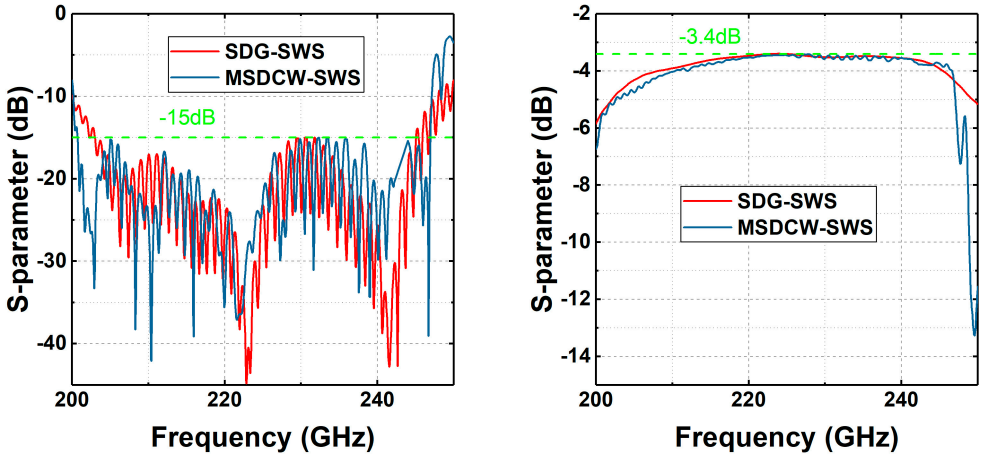

(**a**) (**b**)

Figure 7. (**a**) The S_{11}; (**b**) the S_{21} of MSDCW-TWT and SDG-TWT calculated using CST.

Table 2. Comparison of S parameters of proposed MSDCW-TWT and other TWTs based on SWSs evolved from SDG-SWSs.

Model	Number of Periods of Main SWSs	Frequency Range for S_{11} <−15 dB (GHz)	S_{21}
[19]	10	194~238	<−0.4 dB
[20]	20	180~230	<−1 dB
[28]	37	180~240	>−5 dB (188~255 GHz)
MSDCW-TWT	62	201~247	<−3.4 dB

3.3. Beam–Wave Interaction of the TWTs

The beam–wave interaction simulations of the MSDCW-TWT and SDG-TWT are conducted using CST Particle Studio 2020 in this subsection. Figure 8 shows an output power of ~117 W of the MSDCW-TWT at 220 GHz, which shows that the signal was stable at 10 ns during the interaction simulation process while the output signal amplitude reached 15.3 V (the average output power P in watts was obtained by the output voltage V on the basis of the formula $P = V^2/2$), and the signal of reflection is smaller than the signal of input. The output signal is amplified after ~1 ns because the primary interaction typically needs to be facilitated after the input signal appears in the whole circuit and the electron transit time for the electrons to move to the other end of the system. Figure 9 shows that the frequency spectrum for the output signal is concentrated at 220 GHz. Except for the primary peak at 220 GHz, there are some narrow peaks which are mainly caused by different harmonics at other frequencies with an obviously smaller amplitude than 220 GHz. These results indicate the MSDCW-TWT could stably operate without mode competition or oscillation. Figure 10 displays the phase-space of electrons while the MSDCW-TWT and SDG-TWT reach a steady state. The velocities of most of the electrons are reduced. That means that part of the energy of these electrons is transmitted to waves for signal amplification. The transmitted energy for the MSDCW-TWT is greater than that of the SDG-TWT at 220 GHz.

Figure 11 displays the output power of the TWTs versus the operating frequency. It can be seen from Figure 11 that the maximum output power of ~117 W is obtained at 220 GHz, and the MSDCW-TWT can produce an average output power of more than 58.5 W at 205~239 GHz. The maximum output power of ~79 W is obtained at 245 GHz, and the SDG-TWT can produce an average output power of more than 39.5 W from 206 to 248 GHz. The maximum output power for the MSDCW-TWT is increased by more than 38 W compared to that of the SDG-TWT.

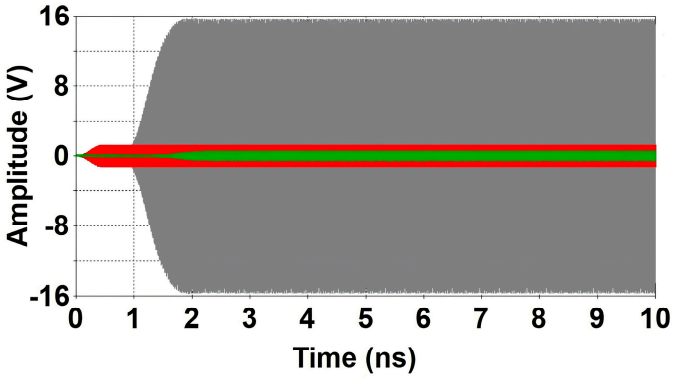

Figure 8. Output signal (gray line), input signal (red line), and reflection signal (green line) for MSDCW-TWT at 220 GHz calculated using CST.

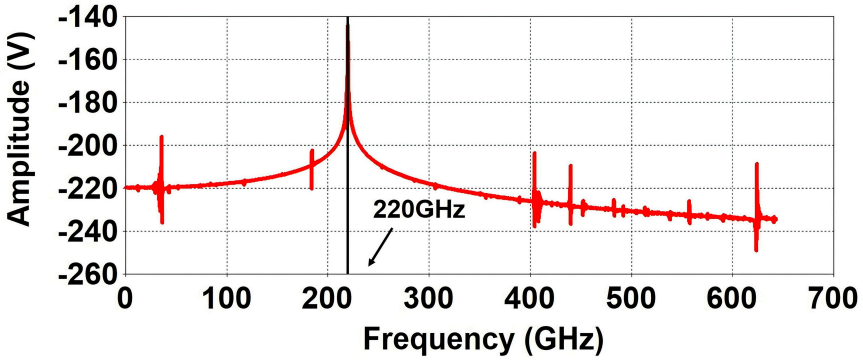

Figure 9. The frequency spectrum of output signal for the MSDCW-TWT calculated using CST.

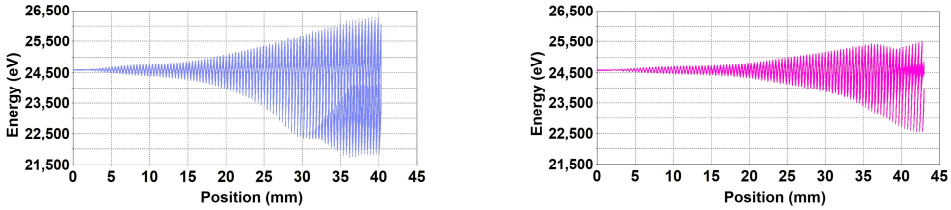

Figure 10. Energy distribution of electrons in phase-space for (**a**) MSDCW-TWT; (**b**) SDG-TWT at 220 GHz calculated using CST.

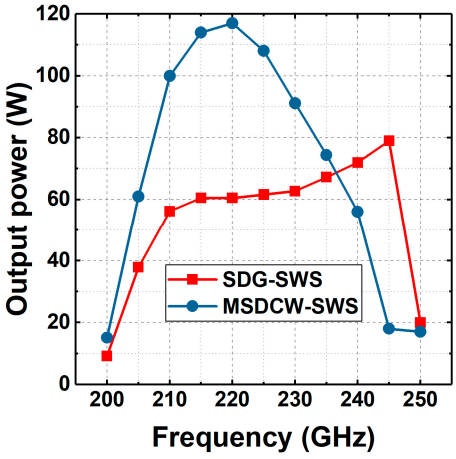

Figure 11. Output power versus operating frequency calculated using CST.

Figure 12a demonstrates the variation in gain with frequency for the MSDCW-TWT and the SDG-TWT. It can be found that the max gains of the MSDCW-TWT and SDG-TWT are 22.11 dB at 220 GHz and 20.4 dB at 245 GHz, respectively. The maximum gain of the MSDCW-TWT is 1.71 dB higher than that of the SDG-TWT. Meanwhile, the variations in electron efficiency with the operating frequency of the two TWTs are given in Figure 12b. It can be observed that the maximum values of electron efficiency for the MSDCW-TWT and the SDG-TWT are 2.64% at 220 GHz and 1.78% at 245 GHz, respectively. The maximum value of the electron efficiency for the MSDCW-TWT is 0.86% higher than that of the SDG-TWT.

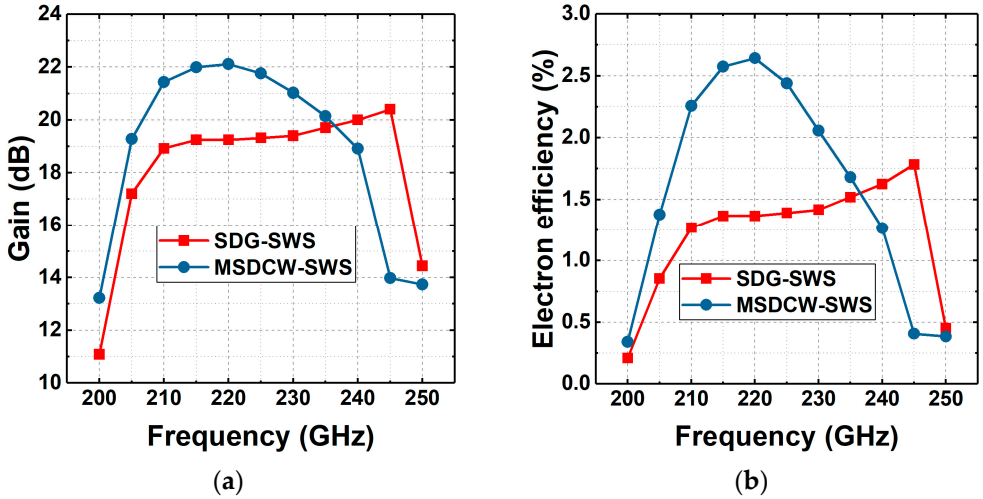

Figure 12. (**a**) Gain versus frequency; (**b**) Electron efficiency versus frequency calculated using CST.

4. Discussion

Based on the above design, optimization, and analysis, the performance parameters of different devices are compared. The MSDCW-SWS has a broad passband of ~90 GHz, a higher interaction impedance of 3.83 ohm at 220 GHz, good coupling and matching performances within 201~247 GHz, a high output power of ~117 W, a high gain of 22.11 dB, and a high electron efficiency of 2.64% at 220 GHz. Possible reasons for these improvements compared with the SDG-TWT are summarized as follows. First, the MSDCW-SWS retained a high coupling impedance from the symmetrical double-grating SWS, as analyzed above. Then, having rows of ridge-loaded gratings, both from the x-direction and the z-direction in Figure 2, increase its *Ez* compared with that of gratings without the added ridges. The most notable improvement brought about by these factors is the increase in the coupling impedance of the MSDCW-SWS, which represents the effective degree of the interaction between the slow-wave system and the electron beam and directly affects the gain and efficiency of the MSDCW-TWT. The higher coupling impedance of the MSDCW-SWS leads to the MSDCW-TWT having a higher output power, higher gain, and higher electron efficiency than the SDG-TWT.

For the TWT, the velocity of electron beam injected is slightly higher than the phase velocity of the EM wave, so most of the electrons give up energy to amplify the EM wave signal and complete the whole beam–wave interaction process. The phase velocity of the slow wave is less than the velocity of light, so that the dispersion curve of the SWS can have a wide, synchronous, and flat frequency range under the premise of a relatively low synchronous voltage. The corrugated structure is also used in other devices such as magnetrons and gyrotrons. The optimum value for a resonator opening was predicted according to the cavitary EM characteristics and obtained for a magnetron in [29]. The tuning of 70 MHz between the $TE_{31,17}$ mode frequency bands was carried out in a gyrotron in [30]. A gyrotron achieves an increase in efficiency and a decrease in velocity spread upon efficiency in [31]. Compared with other devices with a corrugated structure, the MSDCW-TWT simultaneously has the advantages of structural miniaturization, a wide

bandwidth, a high gain, and a low voltage. Table 3 lists important performance parameters of the proposed MSDCW-TWT and other TWTs operating at around 220 GHz in the literature. Compared with the performance parameters of the other TWTs operating at around 220 GHz, the proposed MSDCW-TWT has a higher output power while retaining a high gain and wide band.

Table 3. Comparison of important performance parameters among proposed MSDCW-TWT and other TWTs operating at around 220 GHz.

Model	Frequency (GHz)	Power (W)	Gain (dB)	Passband Width (GHz)
[15]	219	40	33	35
[23]	190	75	18.7	85
[32]	220	66	23	100
[33]	220	28.7	27.6	60
[34]	220	52.1	30.19	80
MSDCW-TWT	220	117	22.11	90

A TWT based on the MSDCW-SWS, which is the core component of the MSDCW-TWT, is a potential and promising THz amplifier that can be applied in the field of radar, space communication, and medical treatment due to its bandwidth characteristics, high power, high gain, and high efficiency. The fabrication, assembly, and testing of the MSDCW-TWT will be performed in the future. Predicted possible problems in these processes include a relatively long fabricating time cycle, errors caused by assembly, and a slight inconformity between simulation and test results caused by test errors, which need to be taken into consideration.

5. Conclusions

In this article, a novel MSDCW-SWS, which is designed for a TWT with a sheet beam, is proposed for the first time. It is proven that the MSDCW-SWS has a higher interaction impedance than the recently proposed SDCW-SWS and the traditional SDG-SWS in a relatively broad frequency band. Interaction simulations of the MSDCW-SWS and the traditional SDG-SWS have also been compared in detail. A TWT based on the MSDCW-SWS has been demonstrated to lead to a greater improvement in output power, gain, and electron efficiency than a TWT based on the SDG-SWS. Simulation results of beam–wave interaction for the MSDCW-TWT show that an output power of more than 58.5 W can be obtained from 205 to 239 GHz, and the maximum power, the maximum gain, and the maximum electron efficiency are 117 W, 22.11 dB, and 2.64% at 220 GHz, respectively. Consequently, the MSDCW-SWS is a potential and promising structure for wideband high-power THz traveling-wave amplifiers.

Author Contributions: Conceptualization, W.G. and S.Y.; Data curation, W.G.; Formal analysis, W.G. and S.Y.; Funding acquisition, W.G.; Investigation, W.G. and S.Y.; Methodology, W.G.; Project administration, W.G.; Resources, W.G.; Software, W.G. and S.Y.; Supervision, S.Y.; Validation, W.G. and S.Y.; Visualization, W.G.; Writing—original draft, W.G.; Writing—review and editing, W.G. and S.Y. All authors have read and agreed to the published version of the manuscript.

Funding: This research received no external funding.

Data Availability Statement: All data included in this study are available upon request by contacting the corresponding author.

Conflicts of Interest: The authors declare no conflicts of interest.

References

1. Siegel, P.H. Terahertz technology. *IEEE Trans. Microw. Theory Tech.* **2002**, *50*, 910–928. [CrossRef]
2. Li, Y.; Chang, C.; Zhu, Z.; Sun, L.; Fan, C. Terahertz Wave Enhances Permeability of the Voltage-Gated Calcium Channel. *J. Am. Chem. Soc.* **2021**, *143*, 4311–4318. [CrossRef] [PubMed]

3. Wu, K.; Qi, C.; Zhu, Z.; Wang, C.; Song, B.; Chang, C. Terahertz Wave Accelerates DNA Unwinding: A Molecular Dynamics Simulation Study. *J. Phys. Chem. Lett.* **2020**, *11*, 7002–7008. [CrossRef] [PubMed]
4. Lyu, N.; Zuo, J.; Zhao, Y.; Zhang, C. Terahertz Synthetic Aperture Imaging with a Light Field Imaging System. *Electronics* **2020**, *9*, 830. [CrossRef]
5. Paoloni, C.; Gamzina, D.; Letizia, R.; Zheng, Y.; Luhmann, N.C., Jr. Millimeter wave traveling wave tubes for the 21st Century. *J. Electromagn. Waves Appl.* **2021**, *35*, 567–603. [CrossRef]
6. Zheng, Y.; Qiu, S.; Griffin, B.; Kowalczyk, R.; Luhmann, N.C., Jr.; Gamzina, D. Compact E-Band Sheet Beam Folded Waveguide Traveling Wave Tube for High Data Rate Communication. *IEEE Trans. Electron Devices* **2023**, *70*, 2508–2513. [CrossRef]
7. Basu, B.N.; Datta, S.K. Microwave tubes and applications. *J. Electromagn. Waves Appl.* **2017**, *31*, 1771–1774. [CrossRef]
8. Minenna, D.F.G.; André, F.; Elskens, Y.; Auboin, J.F.; Doveil, F.; Puech, J.; Duverdier, É. The traveling-wave tube in the history of telecommunication. *Eur. Phys. J. H* **2019**, *44*, 1–36. [CrossRef]
9. Hu, P.; Lei, W.; Jiang, Y.; Huang, Y.; Song, R.; Chen, H.; Dong, Y. Demonstration of a Watt-Level Traveling Wave Tube Amplifier Operating Above 0.3 THz. *IEEE Electron Device Lett.* **2019**, *40*, 973–976. [CrossRef]
10. Cao, L.; He, J.; Huang, M.; Zhang, X.; Zhao, J.; Zhai, D. Design and Performance of a High-Efficiency 120-W Q-Band Space Helix TWT. *IEEE Trans. Plasma Sci.* **2020**, *48*, 658–664. [CrossRef]
11. Wei, W.; Zhong, H.; Wei, Y.; Zhang, L.; Wang, S.; Ge, X.; Dai, R.; Qiu, Z.; Lu, Z.; Wang, W. Investigation of Half Rectangular-Ring Helix Slow Wave Structure for W-Band Wide Bandwidth High-Efficiency TWTs. *IEEE Trans. Plasma Sci.* **2022**, *50*, 4576–4581. [CrossRef]
12. Wu, G.; Wei, Y.; Xu, Z.; Shi, J. Theory and Hot Test of High-Power Broadband Helix Traveling-Wave Tube Based on a Double-Graded Radius and Pitch Circuit. *IEEE Electron Device Lett.* **2021**, *42*, 1868–1870. [CrossRef]
13. Sumathy, M.; Gupta, S.K.; Kumar, B.; Venkateswarlu, Y.; Murthy, C.N.; Santra, M.; Uma Maheswara Reddy, S. Cold Circuit Analysis of a Coupled-Cavity Slow Wave Structure for Mm-Wave TWT. *IEEE Trans. Plasma Sci.* **2020**, *48*, 3024–3029. [CrossRef]
14. Mistretta, A.; Martorana, R.; Bisconti, D.; Muratore, A. Development of a 1.5-kW Average Output Power Coupled-Cavity TWT With a 10% Bandwidth Operating in X-Band. *IEEE Trans. Electron Devices* **2018**, *65*, 2252–2256. [CrossRef]
15. Jiang, Y.; Lei, W.; Hu, P.; Song, R.; Ma, G.; Chen, H.; Jin, X. Demonstration of a 220-GHz Continuous Wave Traveling Wave Tube. *IEEE Trans. Electron Devices* **2021**, *68*, 3051–3055. [CrossRef]
16. Shu, G.; Deng, J.; Xie, L.; Liu, G.; Zhang, L.; Wang, J.; Qian, Z.; He, W. Design, Fabrication, and Cold Test of a High Frequency System for an H-Band Sheet Beam Travelling Wave Tube. *IEEE Trans. Terahertz Sci. Technol.* **2020**, *10*, 292–301. [CrossRef]
17. Lai, J.; Gong, Y.; Xu, X.; Wei, Y.; Duan, Z.; Wang, W.; Feng, J. W-Band 1-kW Staggered Double-Vane Traveling-Wave Tube. *IEEE Trans. Electron Devices* **2012**, *59*, 496–503. [CrossRef]
18. Shu, G.; Wang, J.; Liu, G.; Luo, Y.; Wang, S. An Improved Slow-Wave Structure for the Sheet-Beam Traveling-Wave Tube. *IEEE Trans. Electron Devices* **2016**, *63*, 2089–2096. [CrossRef]
19. Lu, Z.; Wen, R.; Su, Z.; Ge, W.; Wang, Z.; Gong, H.; Gong, Y. Novel Helical Groove Rectangular Waveguide Slow Wave Structure for 0.2 THz Traveling Wave Tube. *IEEE Electron Device Lett.* **2019**, *40*, 1526–1529. [CrossRef]
20. Babaeihaselghobi, A.; Akram, M.N.; Ghavifekr, H.B.; Billa, L.R. A Novel Chevron-Shape Double-Staggered Grating Waveguide Slow Wave Structure for Terahertz Traveling Wave Tubes. *IEEE Trans. Electron Devices* **2020**, *67*, 3781–3787. [CrossRef]
21. Lu, Z.; Gong, Y.; Wei, Y.; Wang, W. Study of the double rectangular waveguide grating slow-wave structure. *Chin. Phys.* **2006**, *15*, 2661–2668. [CrossRef]
22. Lu, Z.; Ge, W.; Wen, R.; Wang, Z.; Gong, H.; Wei, Y.; Gong, Y. 0.2-THz Traveling Wave Tube Based on the Sheet Beam and a Novel Staggered Double Corrugated Waveguide. *IEEE Trans. Plasma Sci.* **2020**, *48*, 3229–3237. [CrossRef]
23. Karetnikova, T.A.; Rozhnev, A.G.; Ryskin, N.M.; Fedotov, A.E.; Mishakin, S.V.; Ginzburg, N.S. Gain Analysis of a 0.2-THz Traveling-Wave Tube with Sheet Electron Beam and Staggered Grating Slow Wave Structure. *IEEE Trans. Electron Devices* **2018**, *65*, 2129–2134. [CrossRef]
24. Shu, G.; Liu, G.; Qian, Z.; He, W. Design, Microfabrication, and Characterization of a Subterahertz-Band High-Order Overmoded Double-Staggered Grating Waveguide for Multiple-Sheet Electron Beam Devices. *IEEE Trans. Electron Devices* **2021**, *68*, 3021–3027. [CrossRef]
25. Baig, A.; Gamzina, D.; Kimura, T.; Atkinson, J.; Domier, C.; Popovic, B.; Himes, L.; Barchfeld, R.; Field, M.; Luhmann, N.C., Jr. Performance of a Nano-CNC Machined 220-GHz Traveling Wave Tube Amplifier. *IEEE Trans. Electron Devices* **2017**, *64*, 2390–2397. [CrossRef]
26. Xie, W.; Wang, Z.; He, F.; Luo, J.; Zhao, D.; Liu, Q. Field theory of a terahertz staggered double-grating arrays waveguide Cerenkov traveling wave amplifier. *Phys. Plasmas.* **2014**, *21*, 043103. [CrossRef]
27. Xie, W.; Wang, Z.-C.; Luo, J.; Liu, Q. Theory and Simulation of Arbitrarily Shaped Groove Staggered Double Grating Array Waveguide. *IEEE Trans. Electron Devices* **2014**, *61*, 1707–1714. [CrossRef]
28. Lu, Z.; Ding, K.; Wen, R.; Ge, W.; Zhu, M.; Wang, Z.; Gong, H.; Gong, Y. Novel Double Tunnel Staggered Grating Slow Wave Structure for 0.2 THz Traveling Wave Tube. *IEEE Electron Device Lett.* **2020**, *41*, 284–287. [CrossRef]
29. Schuenemann, K.; Serebryannikov, A.E.; Sosnytskiy, S.V.; Vavriv, D.M. Optimizing the spatial-harmonic millimeter-wave magnetron. *Phys. Plasmas.* **2003**, *10*, 2559–2565. [CrossRef]
30. Piosczyk, B.; Arnold, A.; Dammertz, G.; Dumbrajs, O.; Kuntze, M.; Thumm, M.K. Coaxial cavity gyrotron—Recent experimental results. *IEEE Trans. Plasma Sci.* **2002**, *30*, 819–827. [CrossRef]

31. Qin, M.; Luo, Y.; Yang, K.; Huang, Y.; Li, H. Numerical study and simulation of a 170 GHz megawatt-level corrugated coaxial-gyrotron. *Vacuum* **2014**, *109*, 34–42. [CrossRef]
32. Titov, V.; Ploskih, A.; Ryskin, N. Study of Beam-Wave Interaction in a Sub-THz Traveling Wave Tube with a Converging Sheet Electron Beam Focused by a Uniform Magnetic Field. *Electronics* **2022**, *11*, 4208. [CrossRef]
33. Deng, G.; Chen, P.; Yang, J.; Yin, Z.; Ruan, J. 0.22 THz two-stage cascaded staggered double-vane traveling-wave tube. *J. Comput. Electron.* **2016**, *15*, 634–638. [CrossRef]
34. Zhang, L.; Wei, Y.; Guo, G.; Ding, C.; Wang, Y.; Jiang, X.; Zhao, G.; Xu, J.; Wang, W.; Gong, Y. A Ridge-Loaded Sine Waveguide for G-Band Traveling-Wave Tube. *IEEE Trans. Plasma Sci.* **2016**, *44*, 2832–2837. [CrossRef]